HHS Public Access

Author manuscript

Acta Biomater. Author manuscript; available in PMC 2018 August 01.

Published in final edited form as:

Acta Biomater. 2017 August ; 58: 291–301. doi:10.1016/j.actbio.2017.05.051.

Tissue and cellular biomechanics during corneal wound injury and repair

Vijay Krishna Raghunathan[§,a,b], **Sara M Thomasy**[§,b,*], **Peter Strøm**[b], **Bernardo Yañez-Soto**[c], **Shaun P Garland**[b], **Jasmyne Sermeno**[b], **Christopher M Reilly**[d], and **Christopher J Murphy**[b,e,*]

[a]The Ocular Surface Institute, College of Optometry, University of Houston, Houston, Texas, United States

[b]Department of Surgical and Radiological Sciences, School of Veterinary Medicine, University of California Davis, Davis, California, United States

[c]CONACYT-Instituto de Fisica, Universidad Autonoma de San Luis Potosi, San Luis Potosi, Mexico

[d]Department of Pathology, Immunology and Microbiology, School of Veterinary Medicine, University of California Davis, Davis, California, United States

[e]Department of Ophthalmology & Vision Sciences, School of Medicine, University of California Davis, Davis, California, United States

Abstract

Corneal wound healing is an enormously complex process that requires the simultaneous cellular integration of multiple soluble biochemical cues, as well as cellular responses to the intrinsic chemistry and biophysical attributes associated with the matrix of the wound space. Here, we document how the biomechanics of the corneal stroma are altered through the course of wound repair following keratoablative procedures in rabbits. Further we documented the influence that substrate stiffness has on stromal cell mechanics.

Following corneal epithelial debridement, New Zealand white rabbits underwent phototherapeutic keratectomy (PTK) on the right eye (OD). Wound healing was monitored using advanced imaging modalities. Rabbits were euthanized and corneas were harvested at various time points following PTK. Tissues were characterized for biomechanics with atomic force microscopy and with histology to assess inflammation and fibrosis. Factor analysis was performed to determine any discernable patterns in wound healing parameters.

The matrix associated with the wound space was stiffest at 7 days post PTK. The greatest number of inflammatory cells were observed 3 days after wounding. The highest number of

[*]**Co-corresponding authors:** Prof. Christopher J Murphy, DVM, Ph.D, DACVO, cjmurphy@ucdavis.edu, Assoc. Prof. Sara M. Thomasy, DVM, PhD, DACVO, smthomasy@ucdavis.edu.

[§]Authors contributed to this work equally and must be considered co-first authors

myofibroblasts and the greatest degree of fibrosis occurred 21 days after wounding. While all clinical parameters returned to normal values 400 days after wounding, the elastic modulus remained greater than pre-surgical values. Factor analysis demonstrated dynamic remodeling of stroma occurs between days 10 and 42 during corneal stromal wound repair.

Elastic modulus of the anterior corneal stroma is dramatically altered following PTK and its changes coincide initially with the development of edema and inflammation, and later with formation of stromal haze and population of the wound space with myofibroblasts. Factor analysis demonstrates strongest correlation between elastic modulus, myofibroblasts, fibrosis and stromal haze thickness, and between edema and central corneal thickness.

1. Introduction

Corneal opacities are one of the leading causes of blindness worldwide [1]. There is an increasing emphasis on the incorporation of biophysical and biochemical stimuli, intrinsic to tissues, for better implant design [2]. Currently available artificial corneas focus on integration of the device into the existing stromal tissue. For this, a part of the native tissue is removed resulting in a wound. However, little is known about how the intrinsic biophysical microenvironment of the cornea is altered during wound healing, and/or how these changes may influence cell differentiation to in turn predict the success of prosthetic integration [3].

Keratoablative surgical procedures such as laser-assisted in situ keratomileusis (LASIK) and photorefractive and phototherapeutic keratectomies (PRK and PTK) that necessitate wounding of the central cornea are widely performed to correct refractive errors and treat anterior stromal disorders [4]. While LASIK largely spares the individual constituents of the anterior cornea, PTK and PRK remove substantial portions of the anterior stroma as well as the epithelium, basement membrane and Bowman’s layer. Renewal of an intact epithelium and basement membrane, replenishment of stromal cells, and precise remodeling of stromal collagen fibers and lamellae are some of the main events that are critical for corneal restoration. Upon corneal stromal wounding, significant remodeling of the stroma occurs, thus altering the microenvironment of the wound space to promote transformation of the quiescent keratocyte to the activated fibroblast and subsequently the differentiated myofibroblast (KFM transformation) [5]. Myofibroblasts also arise from differentiation of bone marrow-derived cells that migrate into the corneal stroma following wounding [6]. These events are orchestrated precisely by cross-talk between biophysical and biochemical stimuli, provided by the remodeling matrix as well as the inflammatory, stromal and epithelial cells in the wound environment [7]. Dysregulation of the wound healing process, such as excessive numbers and/or prolonged persistence of activated fibroblasts and myofibroblasts within the remodeling wound space, can result in the formation of stromal haze or scar formation associated with decreased corneal crystalline expression, increased light scatter and production of disorganized extracellular matrix [8, 9]. In such situations there is reduced corneal transparency that can lead to clinically significant visual compromise.

While the impact of soluble signaling molecules such as transforming growth factor-β (TGF-β) on corneal wound healing processes are well-studied [10, 11], there is a knowledge

gap in regards to the participation of biophysical cues in determining wound healing outcomes. This knowledge gap is particularly relevant due to the expanding use of strategies to stabilize the corneal matrix using cross-linking (CXL) which have been reported to stiffen the corneal matrix [12, 13]. The use of cross-linking was initially motivated by efforts to slow progression of progressive corneal degenerative diseases such as keratoconus [14–16] but its use has expanded to include treatment of numerous corneal diseases including infectious keratitis [17, 18]. Crosslinking is reported to induce anterior keratocyte apoptosis [19–21] and stimulate stromal fibroblast to myofibroblast transformation [19, 21].

We have previously demonstrated that biophysical cues profoundly modulate a host of fundamental corneal cell behaviors that are integral to corneal wound healing including adhesion, migration, proliferation, differentiation and response to growth factors [22–29]. Specifically, we have demonstrated that substratum topography [30] and compliance [31] have a marked effect on fibroblast to myofibroblast transformation and are as potent as TGF-β1, the most well-studied soluble signaling factor affecting corneal stromal cells, in modulating KFM transformation. A better understanding of the biophysical signaling environment that participates in the genesis, persistence and subsequent removal of the myofibroblast within the corneal wound space is critical to identifying new strategies for the management of stromal haze and fibrosis. Here, we report the changes in the corneal biophysical environment over the course of wound healing and the role they play in KFM transformation *in situ*.

2. Materials and Methods

2.1 Animals

The study design was approved by the Institutional Animal Care and Use Committee of the University of California-Davis and performed according to the Association for Research in Vision and Ophthalmology resolution on the use of animals in research. Thirty New Zealand White female rabbits (3 per group Charles River Laboratories, Wilmington, MA) with a mean ± SD body weight and age of 3.6 ± 0.1 kg and 1.2 ± 0.0 years, respectively, were utilized in this study. A complete ophthalmic examination (slit lamp examination & indirect ophthalmoscopy), applanation tonometry (Tonopen XL, Medtronic, Minneapolis, MN, USA), Fourier-domain optical coherence tomography (FD-OCT; RTVue 100, software version 6.1; Optovue Inc., Fremont, CA, USA), ultrasonic pachymetry (Accupach VI; Accutome Ultrasound Inc., Malvern, PA, USA) and fluorescein staining were performed prior to inclusion into the study; only animals free of ocular disease were used. Applanation tonometry and USP were performed following application of 0.5% proparacaine (Alcon Inc., Fort Worth, TX, USA) to the cornea.

2.2 Excimer laser PTK and post-operative treatment

Rabbits were pre-medicated with midazolam (0.7 mg/kg) and hydromorphone (0.1 mg/kg) administered intramuscularly (IM) followed by ketamine (10–30 mg/kg) IM for induction and maintenance of anesthesia. Following administration of proparacaine hydrochloride 0.5% ophthalmic solution (Bausch and Lomb, Rochester, NY, USA), an 8 mm diameter corneal trephine (MSI Instruments, Pheonixville, PA, USA) was used to mark the central

cornea and the epithelium of the right eye (OD) was removed with an excimer spatula (BD Visitec, Franklin Lakes, NJ, USA) within the marked region. An excimer laser (Nidek Excimer Laser Corneal Surgery System EC-5000, Fremont, CA) was used to perform a phototherapeutic keratectomy (PTK) by photoablating the superficial stromal elements of the right cornea (6 mm diameter, 40 Hz, 167 pulses, 100 μm depth) in the center of the epithelial wound. The left eye remained unwounded and served as a control. Rabbits were treated OD with ofloxacin 0.3% ophthalmic solution (Alcon, Hunenberg, Switzerland) twice daily (BID) until re-epithelialization was complete; buprenorphine (0.03–0.06 mg/kg) was administered IM BID for 3–7 days post-wounding to provide analgesia. A slit lamp examination with Modified McDonald-Shadduck scoring, and fluorescein stain was performed daily for the first week post-wounding. A slit lamp examination with Modified McDonald-Shadduck scoring including a semi-quantitative score for stromal haze using a modification of a previously defined system [32], applanation tonometry, FD-OCT, USP, and fluorescein stain were also performed on days 1, 3, 7, 10, 14, 21, 28, 35, 42, and 70 following PTK. Also, a single rabbit was followed for 400 days after wounding.

Fourier-Domain (FD-OCT) imaging (RTVue® 100, software version 6.1; Optovue Inc., Fremont, California, USA; 26000 A scan/sec, 5 μm axial resolution, 840 nm superluminescent diode) of the central cornea was performed using a corneal adaptor module. The RTVue measuring tool was used to measure thickness of the central cornea as well as the thickness of stromal haze, which was observed as a zone of hyper-reflectivity within the anterior stroma, if present (Figure S1).

CCT values in the wounded tissues were compared with baseline values. Presence of edema was scored based on CCT values as follows: none (0): < 85% baseline, mild (1): 85–115% baseline, moderate (2): 116–145% baseline, and severe (3): >145% baseline. These assessments of edema accounted for the removal of stroma from the PTK which resulted in a corneal thickness of ~75% of baseline.

2.3 Tissue harvest and processing

Rabbits were euthanized with pentobarbital (200 mg/kg, IV) and an excimer spatula was used to remove the epithelium OU; the anterior stroma of the left eye was exposed with an excimer laser (6 mm diameter, 40 Hz, 167 pulses, 100 μm depth). For days 28, 42 and 70, an excimer laser was also used to photoablate the anterior basement membrane (ABM) immediately following euthanasia to expose the anterior stroma of the right eye (6 mm diameter, 40 Hz, 25 pulses, 15 μm depth); an EC-5000 calibration card (Nidek Technologies, Gamagori, Japan) was used to protect the opposite half of the cornea where the ABM was already exposed following debridement. An 8 mm central corneal button was harvested from both eyes using a corneal trephine and corneal section scissors. The corneal buttons were divided into four 2 mm sections and stored in Optisol (Chiron Ophthalmics, Irvine, California) at 4° C until AFM measurements were performed within 6 h of euthanasia.

2.4 Atomic force microscopy

Tissue samples were mounted for AFM without any glue and analyses performed as described previously [33–36]. Briefly, elastic modulus was determined in contact mode

using a silicon nitride probe with a square pyramid tip incorporated at the free end (κ=0.32 N/m; PNT-TR-50, Nano and More, Lady's Island, SC); a 5 μm radius borosilicate bead was attached to the pyramid of the cantilever and contact-mode mechanics was determined by obtaining five force-versus-indentation curves at five difference locations of the tissue. This amounted to 25 force curves per sample in each experiment. Using Hertz's model for a spherical indenter, elastic moduli of tissue were determined.

2.5 Immunohistochemistry and histopathology

Corneal buttons, that were not used to determine biomechanics, were formalin fixed, paraffin embedded and sectioned such that 3 sections were mounted per slide. Sections were deparaffinized in xylene, subjected to citrate (pH 6.0) heat induced epitope retrieval, peroxidase blocked and incubated overnight at 4°C with mouse antihuman α-smooth muscle actin (αSMA; Sigma-Aldrich, MO) antibody. Sections were then stained with goat anti-mouse secondary antibody conjugated to AlexaFluor 594 (LifeTechnologies, CA), followed by nuclear counterstaining using DAPI, and cover-slipped. Slides containing the sections from each rabbit (3 rabbits per time point) for every time point (0, 1, 3, 7, 10, 14, 21, 28, 42, 70 days) was imaged along the whole length of the cornea using a Leica DMi8 fluorescence microscope (Leica Microsystems, IL).

Dissected corneas were embedded in paraffin, sectioned (3 sections were mounted per slide), and stained with hemotoxylin and eosin (H&E, FisherScientific, CA) prior to evaluation via light microscopy. All H&E-stained sections were examined by a board certified veterinary pathologist (CMR) who was masked as to group assignments. One slide from each rabbit (3 rabbits per time point) for every time point (0, 1, 3, 7, 10, 14, 21, 28, 42, 70 days) was semi-quantitatively evaluated for severity of fibrosis (0 = none, 1 = mild, 2= moderate, 3 = severe) as well as severity, type, and location of inflammation. Inflammation was assigned a score of 0 when inflammatory cells were absent or there were sparsely scattered individual inflammatory cells. Inflammation was assigned a score of 1 when scattered aggregates or diffusely distributed low numbers of inflammatory cells were observed. Inflammation was assigned a score of 2 when focally large or diffusely moderate numbers of inflammatory cells with or without mild distortion of tissue architecture were observed. Inflammation was assigned a score of 3 when diffuse infiltration or effacement of the mucosa/epithelium by large numbers of inflammatory cells with distortion of tissue architecture was observed. Inflammation was further categorized on the basis of the predominant cell type or types observed (i.e., heterophilic, lymphoplasmacytic, or mixed) within the stroma. Presence or absence of the anterior basement membrane was assessed on 5 micron sections stained with the Periodic-acid Schiff (PAS) technique, which highlights basement membranes.

2.6 Image analysis

For each time point (from 1 to 70 days after wounding), three rabbit corneas were dissected; one cornea was available from a rabbit at 400 days post-wounding. From each corneal sample, 3 sections were mounted per slide and stained for αSMA. Each corneal section in its entirety was fluorescently imaged at 20× using a short working distance APO-PLAN objective with the same exposure setting, and subsequently stitched together. For all images, using a custom MATLAB algorithm, the number of nuclei were counted (from DAPI

channel) to determine total cell numbers. Next, using the αSMA channel information, the outline of each cell was identified if signal intensity was 20% greater than baseline intensity which was determined from negative control slides. The number of αSMA positive cells were thus identified. Data were then expressed as % αSMA positive cells per entire corneal section for each time point.

2.7 Statistical analysis

Data, unless specified otherwise, are presented as mean ± standard deviation (n=3 animals per group). Group wise comparisons were conducted by one-way or two-way ANOVA with post-hoc multiple comparison tests (if $p<0.05$) when appropriate. Collectively all data were pooled into a matrix, and multivariate statistical analyses was conducted as described below:

2.7.1 Principal component and Factor analysis—We performed Principal Component Analysis (PCA) from a data matrix consisting of 54 samples (triplicates of control and wounded for days 1, 3, 7, 10, 14, 21, 28, 42 and 70 days) and 7 variables (elastic modulus, inflammation, fibrosis, edema, number of α-SMA positive cells expressed as % of total number of cells in the stroma, thickness of stromal haze, and central corneal thickness). The data matrix was centered and normalized to obtain a mean value of zero and a standard deviation of 1 for each variable. A 7×7 correlation matrix was calculated from this dataset and the eigenvectors and their corresponding eigenvalues were extracted. The relative percentage of variance of each eigenvalue was quantified and diagramed in a scree plot. The selection of the number of principal components used was performed using the Kaiser-Guttman criteria, using the eigenvectors whose corresponding eigenvalues had a value greater than 1.

The score matrix was calculated by multiplying these eigenvectors by the square root of the corresponding eigenvalue. Following PCA, the score matrix was rotated orthogonally using Varimax to extract the latent factors. The factors loading matrix was obtained from the rotated factor score matrix by matrix operations. The factors were interpreted by associating the variables with highest weights in each factor.

2.8 Fabrication of hydrogels and cell culture

Due to the intrinsic differences in corneal stromal stiffness between rabbits and humans (human stroma stiffer than rabbit at 33 ±6 .1 and 1.1 ± 0.6 kPa respectively) [35, 37] rabbit stromal cells (5000 cells per gel) were cultured on 5 and 25 kPa substrates and human stromal cells were cultured on 25 and 75 kPa substrates to represent softer and stiffer matrix conditions. Polyacrylamide hydrogels with an elastic modulus of 5, 25 and 75 kPa were fabricated as previously described [38]. Primary rabbit corneal stromal cells were isolated as previously described[31] from freshly enucleated young rabbit eyes (Pel-Freeze, Rogers, AR). Primary human corneal stromal cells were isolated as previously described[31] from human donor corneoscleral rims that were unsuitable for transplants (SavingSight, Kansas City, MO). Cells were cultured on the hydrogels, in DMEM low glucose supplemented with 10% FBS and 1% P/S/F, for 3 days in the presence or absence of 10 ng/ml TGFβ1 for rabbit stromal cells or 2 ng/ml TGFβ1 for human stromal cells [31]. Cell mechanics of stromal cells (at least 10 cells per condition, with 5 force curves per cell) cultured on the matrices of

differing stiffness were determined by AFM as previously described [36, 39]. Experiments were performed in triplicate.

3. Results

3.1 Clinical characterization: Central corneal and haze thickness

At least three rabbits were wounded using an excimer laser for each time point from days 1 through 70 and monitored clinically for the entire duration of the study (Figure 1, S2). Prior to wounding, mean central corneal thickness as measured by FD-OCT (CCT; Figure 2a) for the right eye (oculus dexter, OD) for all rabbits was: 359 ± 52 μm (n=30) and did not significantly differ from values obtained in the left eye (oculus sinister, OS; 361 ± 31 μm; n=30; $p = 0.742$). Central corneal thickness OD was maximal 3 days after wounding (486 ± 16 μm, $n = 3$; $p < 0.05$) due to corneal edema then significantly decreased at day 10 after wounding (276 ± 22 μm, $n = 3$, $p < 0.05$) following reformation of an intact epithelium. Central corneal thickness at 70 days after wounding did not significantly differ from baseline values (369 ± 10 μm, $n = 3$, $p = 0.345$). Thickness of the stromal haze, a discrete hyper-reflective zone as measured by FD-OCT in the central cornea, changed over time (Figure 2b, S2). Seven days after wounding, a significant increase in haze was observed (126 ± 40 μm, n=3, $p < 0.05$). Haze, remained significantly elevated up to 70 days (123 ± 66 μm, n=3, $p < 0.05$) after wounding. At 400 days, no haze was observed in the one rabbit, and its CCT was 417 μm.

3.2 Immunohistochemical analyses: Inflammation, fibrosis, and myofibroblasts

Inflammation & fibrosis—Inflammation was observed 1 day after wounding, Figure 3a, 4), and increased in severity up to day 3 before progressively decreasing between days 7 and 21. Inflammation had completely regressed by day 70 and was not observed in the 400 day rabbit. Corneal fibrosis was initially observed at day 7 and significantly increased up to day 21 (Figure 3b) before progressively decreasing up to 70 days after wounding. No fibrosis was observed in the 400 day rabbit.

αSMA positive myofibroblasts—The incidence of myofibroblasts also varied over time (Figure 3c, 4). An initial increase in the number of myofibroblasts was observed 7 days (after wounding, before a brief but significant reduction at days 10 and 14. This was followed by a significant increase in myofibroblast density at days 21 and 28 after wounding, following which the incidence of myofibroblasts dramatically reduced at day 42 (4 ± 5% of cells in stroma) with completely clearing by day 70 post-wounding.

3.3 Elastic modulus of corneal stroma

The elastic modulus of the corneal stroma varied throughout wound healing. The elastic modulus of the unwounded anterior stroma from the left eye of 28 rabbits immediately following photoablation was 0.64 ± 0.35 kPa (mean ± standard deviation; Figure 5). Seven days after wounding, elastic modulus of the anterior stroma was significantly greater at 5.31 ± 2.3 kPa ($p<0.001$). The modulus decreased between days 10 (2.11 ± 0.28 kPa, $p<0.001$) and 14 (1.43 ± 0.33 kPa, $p<0.001$) before increasing significantly at day 21 (3.32 ± 1.27 kPa, $p<0.001$). Subsequently, the modulus reduced at day 28 (1.56 ± 0.97 kPa, $p<0.05$) before

increasing to 2.47 ± 0.58 kPa ($p<0.001$) at day 42, and finally reducing to 1.64 ± 0.39 kPa ($p<0.001$) at day 70. The elastic modulus of the stroma for one rabbit at 400 days post-wounding remained mildly elevated at 1.48 ± 1.04 kPa.

Elastic moduli of the basement membrane at days 28, 42, and 70 were also determined (Figure S3). PAS staining demonstrated a complete BM at day 28, before being uniform and thicker at days 42 and 70 (data not shown). Modulus of the BM on day 28 was lower in the wounded corneas (1.622 ± 0.12 kPa) than control corneas (6.71 ± 0.36 kPa) and progressively increased on days 42 (4.94 ± 0.54 kPa) and 70 (7.30 ± 0.57 kPa).

3.4 Multivariate factor analysis

Principal component analysis demonstrated that greater than 70% of the variance in data could be explained from the first two principal components. Six of the seven variables contributed to over 70% of the variation (table 1, table S1); the contribution of inflammation to the variance was less than 70% was thus excluded from the analysis. Therefore, we used the first two components to perform matrix rotation and factor analysis. Using the varimax method for rotation to maximize the sum of variance for squared loadings, we determined the relationship between the two factors and the variable scores (table 1, Figure S4). Using the scores obtained from the varimax method, the loadings matrix was determined for each rabbit at the various time points (Figure 6). The distribution and correlation of these variables, when analyzed together, is represented as a scores plot in Figure S5. The cosine of the angle between variables indicated correlation between them and is now listed in table S2.

3.5 Effect of substratum stiffness on cell mechanics

The elastic modulus of human and rabbit corneal stromal cells significantly increased with increasing substratum stiffness as well as in the presence of TGFβ1 treatment (Figure 7).

4. Discussion

Here, we document progressive alteration in the mechanical attributes of the stromal wound space throughout wound healing and correlate changes in matrix stiffness with the presence of αSMA positive myofibroblasts, inflammation, fibrosis, and clinical parameters such as edema, central corneal thickness and stromal haze thickness using a multivariate model. We observed **(i)** stromal edema immediately following wounding, **(ii)** early inflammation that gradually reduced with time, **(iii)** elevated stiffness of the anterior corneal stroma that precedes significant upregulation of myofibroblasts, **(iv)** that this stiffness never returns to pre-surgical values, and **(v)** stromal cells treated with TGFβ1 *in vitro* are inherently stiffer than untreated cells, and that their stiffness is significantly determined by the underlying substratum stiffness. Collectively, our results demonstrate that matrix stiffness of the corneal wound microenvironment changes throughout wound healing and that these changes may in turn modulate subsequent cellular mechanics.

Immediately after and for up to 3 days post-wounding, maximal stromal edema was observed as evidenced by increased central corneal thickness due to disruption of the epithelial barrier [40, 41]. Re-establishment of an intact epithelium was observed at day 7 after wounding in 95% of rabbits. These are consistent with previous studies that

demonstrated re-establishment of an intact epithelium is critical for wound healing [42, 43]. One report suggests that injury to the epithelium results in the recruitment of platelets and may be a necessary event for re-epithelialization [44]. We observed mild inflammation within 24 h of wounding that peaked between 3 and 7 days post-wounding before progressively declining. The recruitment of platelets and other inflammatory cells results in the secretion of numerous cytokines and growth factors that trigger downstream effects. Although both edema and inflammation were observed in our study, multivariate analyses demonstrated that edema contributed significantly to the dynamic remodeling-trend observed during the repair process with surprisingly little effect from inflammation.

Next, we determined the advent of myofibroblasts in the corneal stroma post-PRK. Myofibroblasts are major contributors to corneal opacity with reduced expression of crystallins (proteins responsible for corneal transparency)[8], greater secretion of type III collagen and a ‘spread’ morphology[45, 46]. Contractile myofibroblasts appeared in the anterior stroma within a week of wounding, with maximal presence 3–4 weeks post wounding. In fact, the persistence of myofibroblasts in the sub-epithelial region is thought to result in haze development after photorefractive keratectomy [47, 48]. Maximal inflammation and occurrence of sub-epithelial myofibroblasts was documented on day 3 ahead of maximal stiffness of the anterior stroma on day 7. *Importantly, this increase in stiffness preceded the peak occupation of myofibroblasts in the anterior stroma*. We have demonstrated previously that, stiffer substrates promote myofibroblast differentiation *in vitro*[31]. These findings suggest that the increase in wound space matrix stiffness plays a significant role in promoting KFM transformation. A previous report detailing the repair process in transcorneal freeze stromal wounds in NZW rabbits, documented matrix reorganization within 3 days of wounding, significant increases in stromal thickness 7–14 days post wounding, and minimal haze at 28 days [49]. An important study by Netto et al demonstrated that photoablative wounds >−9.0 D, similar to the photoablation of 100 μm in the present study, resulted in significant haze even 4 weeks after wounding [50]. In our study, histologic evidence (data not shown) demonstrated reformation of a complete BM at day 28 in the wounded corneas, accompanied by significant haze. Accompanying this, we observed that the elastic modulus of the BM at day 42 was the same stiffness as a normal BM [35]. Considering the elastic modulus of the BM increases steadily from days 28 to 42, data strongly suggest that the mechanical properties of the BM vary with time as they are replenished. These dynamically changing properties of the BM further influence epithelial cell behavior as supported by a number of studies *in vitro* [22–24, 51]. Further, the dramatic drop in the number of myofibroblasts observed at day 42 suggests that restoration of the BM in corneal stromal wounds plays a role in the life cycle of myofibroblasts in stromal wounds. It is plausible that a more permeable epithelial-stromal interface exists until the formation of an intact BM and this contributes potently to the dynamic relationship between the corneal epithelium and stroma during the remodeling phase of wound repair.

We documented the time dependent changes in the clinical, histologic, and mechanical parameters. The variance in- and between all measured parameters over time were analyzed using multivariate statistics to determine trends, if any, during the wound repair process. Our data demonstrated that a clear pattern emerged throughout wound repair. An increase in inflammatory cells occurred up to 3 days post-photoablation, following which the stroma

became thinner, stiffer, and the number of myofibroblasts increased. Between days 14 and 28, dynamic changes occurred in all measured parameters demonstrating the complexity of active remodeling of the corneal stroma during repair. Notably, reciprocal changes in elastic moduli, myofibroblast presence, and histologic fibrosis were all prevalent during this period. These were followed by the corneal stroma returning to pre-surgical state for almost all parameters except for the elastic modulus suggesting durable modifications in the biophysical attributes of the stroma. We acknowledge that there are temporal and phenotypic differences in rabbit and human stromal wound repair as well as disparity in normal corneal structure and biomechanics between the two species [35, 37, 52]. Nonetheless, the changes in corneal biomechanics associated with corneal wounding identified in the present study are suggestive of a generalizable process. Our findings support pursuing subsequent studies in nonhuman primate possessing a cornea that more closely mimics that of humans [53].

Incidence of myofibroblasts along *aligned* collagen bundles 2 weeks post photoablation have been reported [50, 54, 55] suggesting their participation in stromal remodeling. In this study, although we did not document changes in collagen fibril organization at the various time points, we recognize that it likely plays a significant role in the recorded modulation of corneal biomechanics [49, 56] and provide the platform for migration of fibroblasts/myofibroblasts during healing [5, 54, 57]. Previously, we have reported soft substrates and topographically patterned substrates stabilized the fibroblast phenotype, inhibiting myofibroblast transdifferentiation (even in the presence of TGFβ1), while planar substrates and stiff substrates promoted transformation into the myofibroblast phenotype [27, 30, 31]. This observation is particularly relevant given that crosslinking with riboflavin, which dramatically stiffens the cornea, is increasingly being used to treat a myriad of conditions including keratoconus and infectious keratitis [58, 59]. It is thus plausible that a stiff cornea which is subsequently wounded may experience excessive KFM transformation and concomitant stromal haze.

Our results also document that myofibroblasts are inherently stiffer than keratocytes. We also found that the intrinsic stiffness of keratocytes and myofibroblasts are greater when cultured on stiffer substrates. Taking into consideration that changes in corneal mechanics do not revert to pre-surgical values during the timespan of these experiments, we speculate that any subsequent injury to the cornea may promote genesis of contractile myofibroblasts that may, in turn, increase the incidence of haze resulting in a positive feedback loop. Long-term studies will be required to confirm/refute this hypothesis. These results collectively allow us to posit that the *early appearance of myofibroblasts are a result of inflammatory response that is sustained due to an increased permeable epithelial-stromal interface associated with removal of the anterior basement membrane and disruption of epithelial integrity. The occurrence of increasing numbers of contractile myofibroblasts at later time-points may be a direct result of early increases in stromal stiffness. It is possible that alterations in matrix and stromal cell mechanics participate in directing the entire lifecycle of the myofibroblast in the wound space, from appearance through removal.*

5. Summary

Elastic modulus of the anterior corneal stroma is dramatically altered following PTK and correlates initially with the development of edema and inflammation, and later with formation of stromal haze and population of the wound space with myofibroblasts. Factor analysis suggests that there are strong correlation between **(i)** increased elastic modulus, haze, fibrosis, and incidence of myofibroblasts, and **(ii)** between edema and central corneal thickness. Importantly, to our knowledge, this is the first study to document a relationship between elastic modulus with clinical and histologic parameters over the course of wound healing. Future studies will be required to determine the causal relationship (if any) between each clinical/histologic parameter with elastic modulus. With emerging engineering approaches for modulating corneal biomechanics such as crosslinking with riboflavin and hyaluronidase to stiffen or soften the stroma, respectively, it is critical to better understand the long-term consequences of changing the biophysical characteristics of the corneal stroma.

Supplementary Material

Refer to Web version on PubMed Central for supplementary material.

Acknowledgments

Supported by National Institutes of Health Grants R01EY016134, R01EY019970, K08EY021142, and P30EY12576 and by an unrestricted grant from Research to Prevent Blindness. VKR was supported partially by start-up funds at UHCO.

References

1. Whitcher JP, Srinivasan M, Upadhyay MP. Corneal blindness: a global perspective. Bull. World Health Organ. 2001; 79(3):214–21. [PubMed: 11285665]
2. Sima LE. Extracellular Signals for Guiding Mesenchymal Stem Cells Osteogenic Fate. Curr. Stem Cell Res. Ther. 2017; 12(2):139–144. [PubMed: 26496887]
3. Murphy CJ, Nealey PF, Gasiorowski JZ. Biophysical Cues and Cell Behavior: The Big Impact of Little Things. Annu. Rev. Biomed. Eng. 2013; 15(1) null.
4. Sandoval HP, Donnenfeld ED, Kohnen T, Lindstrom RL, Potvin R, Tremblay DM, Solomon KD. Modern laser in situ keratomileusis outcomes. J. Cataract Refract. Surg. 2016; 42(8):1224–34. [PubMed: 27531300]
5. Myrna KE, Pot SA, Murphy CJ. Meet the corneal myofibroblast: the role of myofibroblast transformation in corneal wound healing and pathology. Vet. Ophthalmol. 2009; 12:25–27. [PubMed: 19891648]
6. Barbosa FL, Chaurasia SS, Cutler A, Asosingh K, Kaur H, de Medeiros FW, Agrawal V, Wilson SE. Corneal myofibroblast generation from bone marrow-derived cells. Exp. Eye Res. 2010; 91(1):92–6. [PubMed: 20417632]
7. Torricelli AA, Wilson SE. Cellular and extracellular matrix modulation of corneal stromal opacity. Exp. Eye Res. 2014; 129(0):151–60. [PubMed: 25281830]
8. Jester JV, Moller-Pedersen T, Huang J, Sax CM, Kays WT, Cavangh HD, Petroll WM, Piatigorsky J. The cellular basis of corneal transparency: evidence for 'corneal crystallins'. J. Cell Sci. 1999; 112(Pt 5):613–22. [PubMed: 9973596]
9. Jester JV, Budge A, Fisher S, Huang J. Corneal Keratocytes: Phenotypic and Species Differences in Abundant Protein Expression and In Vitro Light-Scattering. Invest. Ophthalmol. Vis. Sci. 2005; 46(7):2369–2378. [PubMed: 15980224]

10. Tandon A, Tovey JC, Sharma A, Gupta R, Mohan RR. Role of transforming growth factor Beta in corneal function, biology and pathology. Curr. Mol. Med. 2010; 10(6):565–78. [PubMed: 20642439]
11. Saika S. TGFbeta pathobiology in the eye. Lab. Invest. 2006; 86(2):106–15. [PubMed: 16341020]
12. Cherfan D, Verter EE, Melki S, Gisel TE, Doyle FJ Jr, Scarcelli G, Yun SH, Redmond RW, Kochevar IE. Collagen cross-linking using rose bengal and green light to increase corneal stiffness. Invest. Ophthalmol. Vis. Sci. 2013; 54(5):3426–33. [PubMed: 23599326]
13. Tomkins O, Garzozi HJ. Collagen cross-linking: Strengthening the unstable cornea. Clin. Ophthalmol. 2008; 2(4):863–867. [PubMed: 19668440]
14. Wollensak G, Iomdina E. Long-term biomechanical properties of rabbit sclera after collagen crosslinking using riboflavin and ultraviolet A (UVA). Acta Ophthalmol. 2009; 87(2):193–8. [PubMed: 18803623]
15. Wollensak G, Iomdina E. Crosslinking of scleral collagen in the rabbit using glyceraldehyde. J. Cataract Refract. Surg. 2008; 34(4):651–6. [PubMed: 18361989]
16. Wollensak G, Spoerl E, Seiler T. Stress-strain measurements of human and porcine corneas after riboflavin-ultraviolet-A-induced cross-linking. J. Cataract Refract. Surg. 2003; 29(9):1780–5. [PubMed: 14522301]
17. Tayapad JB, Viguilla AQ, Reyes JM. Collagen cross-linking and corneal infections. Curr. Opin. Ophthalmol. 2013; 24(4):288–90. [PubMed: 23703462]
18. Makdoumi K, Mortensen J, Crafoord S. Infectious keratitis treated with corneal crosslinking. Cornea. 2010; 29(12):1353–8. [PubMed: 21102196]
19. Mastropasqua L, Nubile M, Calienno R, Mattei PA, Pedrotti E, Salgari N, Mastropasqua R, Lanzini M. Corneal cross-linking: intrastromal riboflavin concentration in iontophoresis-assisted imbibition versus traditional and transepithelial techniques. Am. J. Ophthalmol. 2014; 157(3):623–30. e1. [PubMed: 24321474]
20. Salomao MQ, Chaurasia SS, Sinha-Roy A, Ambrosio R Jr, Esposito A, Sepulveda R, Agrawal V, Wilson SE. Corneal wound healing after ultraviolet-A/riboflavin collagen cross-linking: a rabbit study. J. Refract. Surg. 2011; 27(6):401–7. [PubMed: 21162471]
21. Esquenazi S, He J, Li N, Bazan HE. Immunofluorescence of rabbit corneas after collagen cross-linking treatment with riboflavin and ultraviolet A. Cornea. 2010; 29(4):412–7. [PubMed: 20164740]
22. Fraser SA, Ting YH, Mallon KS, Wendt AE, Murphy CJ, Nealey PF. Submicron and nanoscale feature depth modulates alignment of stromal fibroblasts and corneal epithelial cells in serum-rich and serum-free media. J. Biomed. Mater. Res. A. 2008; 86(3):725–35. [PubMed: 18041718]
23. Tocce EJ, Smirnov VK, Kibalov DS, Liliensiek SJ, Murphy CJ, Nealey PF. The ability of corneal epithelial cells to recognize high aspect ratio nanostructures. Biomaterials. 2010; 31(14):4064–72. [PubMed: 20153044]
24. Karuri NW, Liliensiek S, Teixeira AI, Abrams G, Campbell S, Nealey PF, Murphy CJ. Biological length scale topography enhances cell-substratum adhesion of human corneal epithelial cells. J. Cell Sci. 2004; 117(Pt 15):3153–64. [PubMed: 15226393]
25. Karuri NW, Porri TJ, Albrecht RM, Murphy CJ, Nealey PF. Nano- and microscale holes modulate cell-substrate adhesion, cytoskeletal organization, and - beta1 integrin localization in SV40 human corneal epithelial cells. IEEE Trans Nanobioscience. 2006; 5(4):273–80. [PubMed: 17181027]
26. Liliensiek SJ, Campbell S, Nealey PF, Murphy CJ. The scale of substratum topographic features modulates proliferation of corneal epithelial cells and corneal fibroblasts. J. Biomed. Mater. Res. A. 2006; 79(1):185–92. [PubMed: 16817223]
27. Pot SA, Liliensiek SJ, Myrna KE, Bentley E, Jester JV, Nealey PF, Murphy CJ. Nanoscale topography-induced modulation of fundamental cell behaviors of rabbit corneal keratocytes, fibroblasts, and myofibroblasts. Invest. Ophthalmol. Vis. Sci. 2010; 51(3):1373–81. [PubMed: 19875665]
28. Yanez-Soto B, Liliensiek SJ, Murphy CJ, Nealey PF. Biochemically and topographically engineered poly(ethylene glycol) diacrylate hydrogels with biomimetic characteristics as substrates for human corneal epithelial cells. J. Biomed. Mater. Res. A. 2013; 101(4):1184–94. [PubMed: 23255502]

29. Yanez-Soto B, Liliensiek SJ, Gasiorowski JZ, Murphy CJ, Nealey PF. The influence of substrate topography on the migration of corneal epithelial wound borders. Biomaterials. 2013; 34(37): 9244–51. [PubMed: 24016856]
30. Myrna KE, Mendonsa R, Russell P, Pot SA, Liliensiek SJ, Jester JV, Nealey PF, Brown D, Murphy CJ. Substratum topography modulates corneal fibroblast to myofibroblast transformation. Invest. Ophthalmol. Vis. Sci. 2012; 53(2):811–6. [PubMed: 22232431]
31. Dreier B, Thomasy SM, Mendonsa R, Raghunathan VK, Russell P, Murphy CJ. Substratum compliance modulates corneal fibroblast to myofibroblast transformation. Invest. Ophthalmol. Vis. Sci. 2013; 54(8):5901–7. [PubMed: 23860754]
32. Fantes FE, Hanna KD, Waring GO 3rd, Pouliquen Y, Thompson KP, Savoldelli M. Wound healing after excimer laser keratomileusis (photorefractive keratectomy) in monkeys. Arch. Ophthalmol. 1990; 108(5):665–75. [PubMed: 2334323]
33. Morgan JT, Raghunathan VK, Thomasy SM, Murphy CJ, Russell P. Robust and artifact-free mounting of tissue samples for atomic force microscopy. BioTechniques. 2014; 56(1):40–2. [PubMed: 24447138]
34. McKee CT, Last JA, Russell P, Murphy CJ. Indentation versus tensile measurements of Young's modulus for soft biological tissues. Tissue engineering. Part B, Reviews. 2011; 17(3):155–64. [PubMed: 21303220]
35. Thomasy SM, Raghunathan VK, Winkler M, Reilly CM, Sadeli AR, Russell P, Jester JV, Murphy CJ. Elastic modulus and collagen organization of the rabbit cornea: epithelium to endothelium. Acta Biomater. 2014; 10(2):785–91. [PubMed: 24084333]
36. Chang YR, Raghunathan VK, Garland SP, Morgan JT, Russell P, Murphy CJ. Automated AFM force curve analysis for determining elastic modulus of biomaterials and biological samples. J Mech Behav Biomed Mater. 2014; 37(0):209–18. [PubMed: 24951927]
37. Last JA, Thomasy SM, Croasdale CR, Russell P, Murphy CJ. Compliance profile of the human cornea as measured by atomic force microscopy. Micron. 2012; 43(12):1293–8. [PubMed: 22421334]
38. Wood JA, Shah NM, McKee CT, Hughbanks ML, Liliensiek SJ, Russell P, Murphy CJ. The role of substratum compliance of hydrogels on vascular endothelial cell behavior. Biomaterials. 2011; 32(22):5056–64. [PubMed: 21501863]
39. McKee CT, Wood JA, Shah NM, Fischer ME, Reilly CM, Murphy CJ, Russell P. The effect of biophysical attributes of the ocular trabecular meshwork associated with glaucoma on the cell response to therapeutic agents. Biomaterials. 2011; 32(9):2417–23. [PubMed: 21220171]
40. Dohlman CH. The function of the corneal epithelium in health and disease. The Jonas S. Friedenwald Memorial Lecture. Invest. Ophthalmol. 1971; 10(6):383–407. [PubMed: 4325305]
41. Dohlman CH, Gasset AR, Rose J. The effect of the absence of corneal epithelium or endothelium on the stromal keratocytes. Invest. Ophthalmol. Vis. Sci. 1968; 7(5):520–534.
42. Suzuki K, Tanaka T, Enoki M, Nishida T. Coordinated reassembly of the basement membrane and junctional proteins during corneal epithelial wound healing. Invest. Ophthalmol. Vis. Sci. 2000; 41(9):2495–500. [PubMed: 10937559]
43. Nakamura K, Kurosaka D, Bissen-Miyajima H, Tsubota K. Intact corneal epithelium is essential for the prevention of stromal haze after laser assisted in situ keratomileusis. Br. J. Ophthalmol. 2001; 85(2):209–213. [PubMed: 11159488]
44. Li Z, Rumbaut RE, Burns AR, Smith CW. Platelet Response to Corneal Abrasion Is Necessary for Acute Inflammation and Efficient Re-epithelialization. Invest. Ophthalmol. Vis. Sci. 2006; 47(11): 4794–4802. [PubMed: 17065490]
45. Petroll WM, Miron-Mendoza M. Mechanical interactions and crosstalk between corneal keratocytes and the extracellular matrix. Exp. Eye Res. 2015; 133(0):49–57. [PubMed: 25819454]
46. Wilson SE. Corneal myofibroblast biology and pathobiology: Generation, persistence, and transparency. Exp. Eye Res. 2012; 99(0):78–88. [PubMed: 22542905]
47. Shah SS, Kapadia MS, Meisler DM, Wilson SE. Photorefractive keratectomy using the summit SVS Apex laser with or without astigmatic keratotomy. Cornea. 1998; 17(5):508–16. [PubMed: 9756445]

48. Siganos DS, Katsanevaki VJ, Pallikaris IG. Correlation of subepithelial haze and refractive regression 1 month after photorefractive keratectomy for myopia. J. Refract. Surg. 1999; 15(3): 338–42. [PubMed: 10367577]

49. Petroll WM, Kivanany PB, Hagenasr D, Graham EK. Corneal Fibroblast Migration Patterns During Intrastromal Wound Healing Correlate With ECM Structure and AlignmentFibroblast Patterning During Intrastromal Migration. Invest. Ophthalmol. Vis. Sci. 2015; 56(12):7352–7361. [PubMed: 26562169]

50. Netto MV, Mohan RR, Sinha S, Sharma A, Dupps W, Wilson SE. Stromal haze, myofibroblasts, and surface irregularity after PRK. Exp. Eye Res. 2006; 82(5):788–797. [PubMed: 16303127]

51. Dreier B, Raghunathan VK, Russell P, Murphy CJ. Focal adhesion kinase knockdown modulates the response of human corneal epithelial cells to topographic cues. Acta Biomater. 2012; 8(12): 4285–94. [PubMed: 22813850]

52. Winkler M, Shoa G, Tran ST, Xie Y, Thomasy S, Raghunathan VK, Murphy C, Brown DJ, Jester JV. A Comparative Study of Vertebrate Corneal Structure: The Evolution of a Refractive Lens. Invest. Ophthalmol. Vis. Sci. 2015; 56(4):2764–72. [PubMed: 26066606]

53. Melles GR, Binder PS, Beekhuis WH, Wijdh RH, Moore MN, Anderson JA, SundarRaj N. Scar tissue orientation in unsutured and sutured corneal wound healing. The British Journal of Ophthalmology. 1995; 79(8):760–765. [PubMed: 7547789]

54. Farid M, Morishige N, Lam L, Wahlert A, Steinert RF, Jester JV. Detection of corneal fibrosis by imaging second harmonic-generated signals in rabbit corneas treated with mitomycin C after excimer laser surface ablation. Invest. Ophthalmol. Vis. Sci. 2008; 49(10):4377–83. [PubMed: 18502995]

55. Chaurasia SS, Kaur H, de Medeiros FW, Smith SD, Wilson SE. Reprint of “Dynamics of the expression of intermediate filaments vimentin and desmin during myofibroblast differentiation after corneal injury”. Exp. Eye Res. 2009; 89(4):590–596. [PubMed: 19747592]

56. Petroll WM, Lakshman N. Fibroblastic Transformation of Corneal Keratocytes by Rac Inhibition is Modulated by Extracellular Matrix Structure and Stiffness. J Funct Biomater. 2015; 6(2):222–240. [PubMed: 25874856]

57. Petroll WM, Cavanagh HD, Jester JV. Dynamic three-dimensional visualization of collagen matrix remodeling and cytoskeletal organization in living corneal fibroblasts. Scanning. 2004; 26(1):1–10. [PubMed: 15000286]

58. Snibson GR. Collagen cross-linking: a new treatment paradigm in corneal disease - a review. Clin Exp Ophthalmol. 2010; 38(2):141–53. [PubMed: 20398104]

59. Alio JL, Abbouda A, Valle DD, del Castillo JMB, Fernandez JAG. Corneal cross linking and infectious keratitis: a systematic review with a meta-analysis of reported cases. Journal of Ophthalmic Inflammation and Infection. 2013; 3(1):47. [PubMed: 23718849]

Statement of significance

Tissue biomechanics during the course of corneal wound healing is documented for the first time through atomic force microscopy, and is correlated with advanced clinical imaging and immunohistochemistry. Parameters obtained from the study are applied in a multivariate statistical model to cluster the data for better classification and monitor the wound repair process. Elastic modulus of the anterior corneal stroma is dramatically altered following wounding and correlates initially with the development of edema and inflammation, and later with formation of stromal haze and population of the wound space with myofibroblasts. Importantly, the occurrence of myofibroblasts is preceded by changes in tissue mechanics, which is important to consider in light of crosslinking procedures applied to treat corneal diseases.

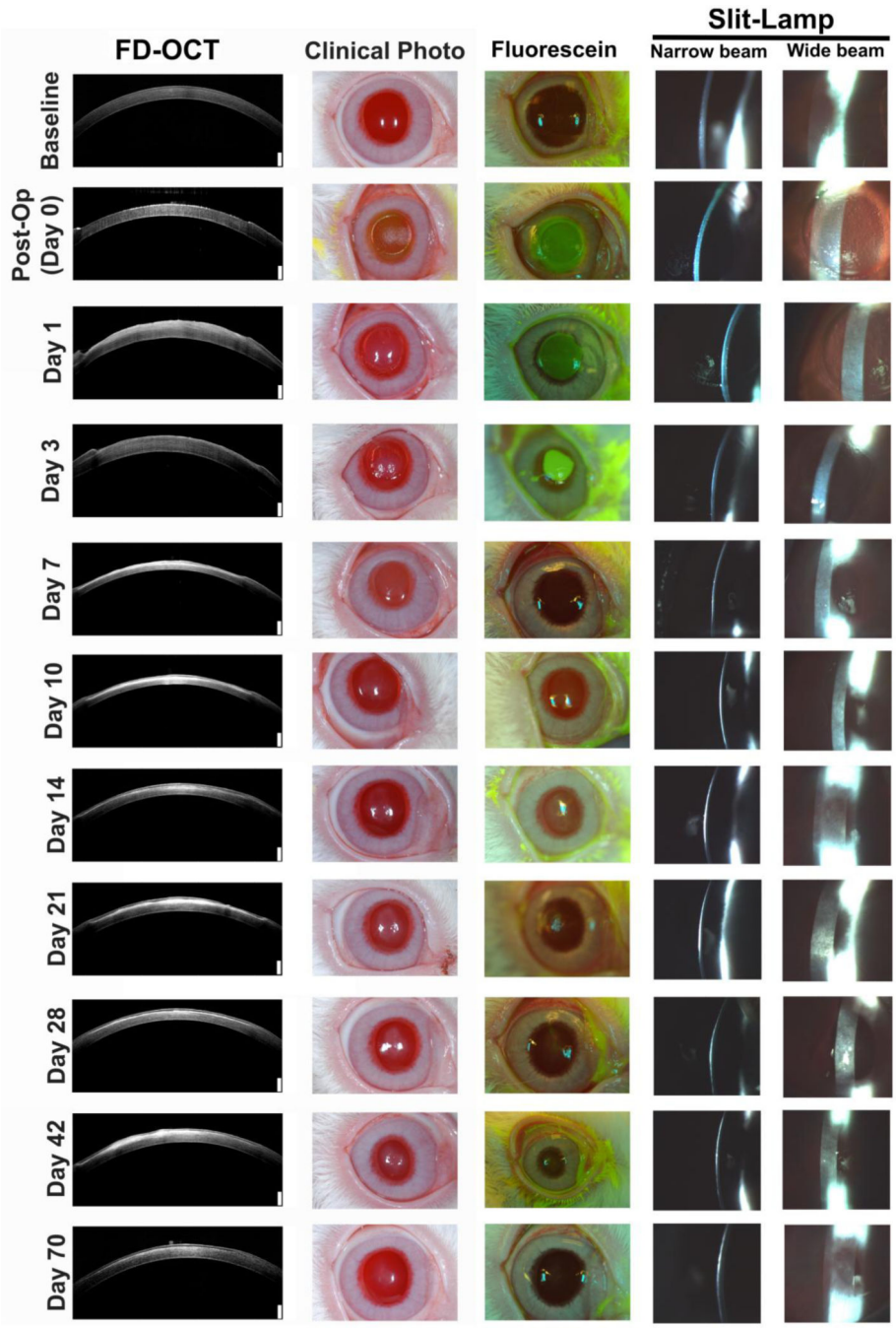

Figure 1.

Haze is observed in both FD-OCT and clinical images. NZW rabbits were wounded with an excimer laser and followed clinically through 70 days. Hyper-reflective areas in FD-OCT images corresponded to haze and was correlated with clinical color photographs. At least 3 rabbits were imaged for each time point. White scale bar in FD-OCT images are 250 μm.

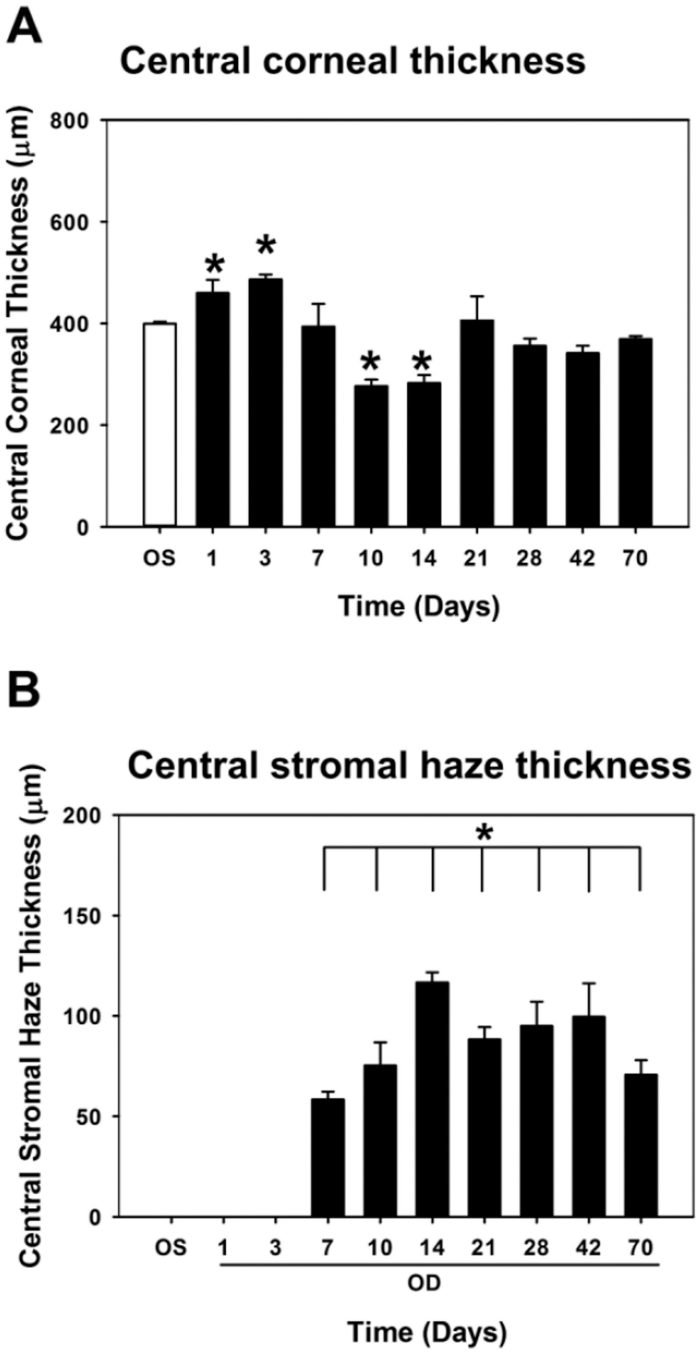

Figure 2.

Variation in central corneal thickness (CCT) and stromal haze thickness throughout wound healing as measured by FD-OCT. **(A)** CCT was greatest 1 day after wounding before progressively declining. **(B)** Corneal stromal haze thickness progressively increased between day 7 and day 14, before declining slightly at 70 days. Data are mean ± standard error in mean. Asterisks indicate statistically significant differences compared with unwounded eye (OS). *$p<0.05$, one-way ANOVA, followed by Dunnett's multiple comparison test compared with OS.

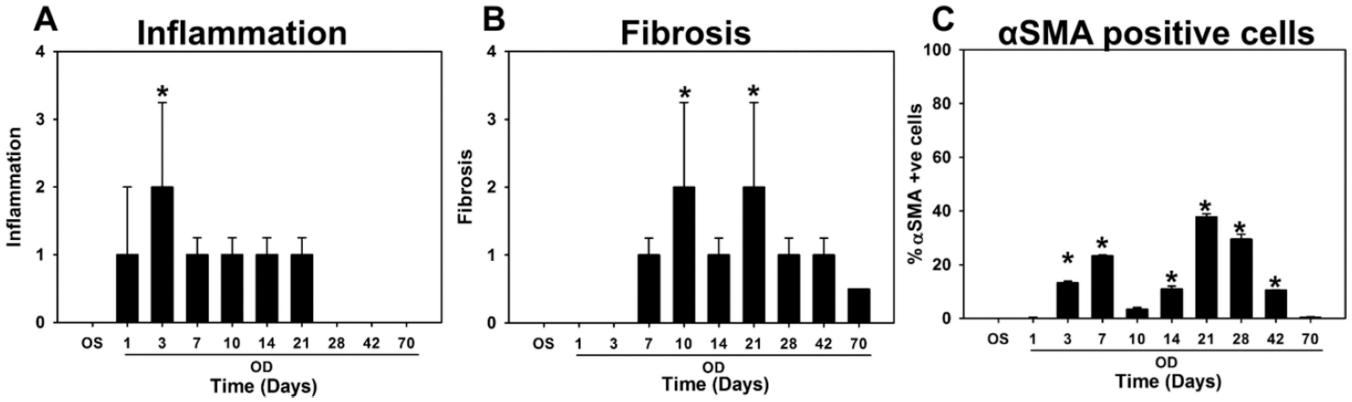

Figure 3.

Inflammation, fibrosis and myofibroblast number vary throughout wound healing. **(A)** Inflammation was greatest 3 days after wounding, and **(B)** Fibrosis was maximum 10 and 21 days after wounding. Scores presented are semi-quantitative measures as analyzed by a board-certified veterinary pathologist. **(C)** Percentage of αSMA positive cells (myofibroblasts) were determined from images after immunohistochemical staining for αSMA. The greatest number of myofibroblasts were present 21 and 28 days after wounding before disappearing by 42 days. Data for inflammation and fibrosis are median ± 75%/25% quartile, and for αSMA are mean ± SD. *$p<0.05$, one-way ANOVA on Ranks, followed by Dunnett's multiple comparison test compared with findings from control eyes.

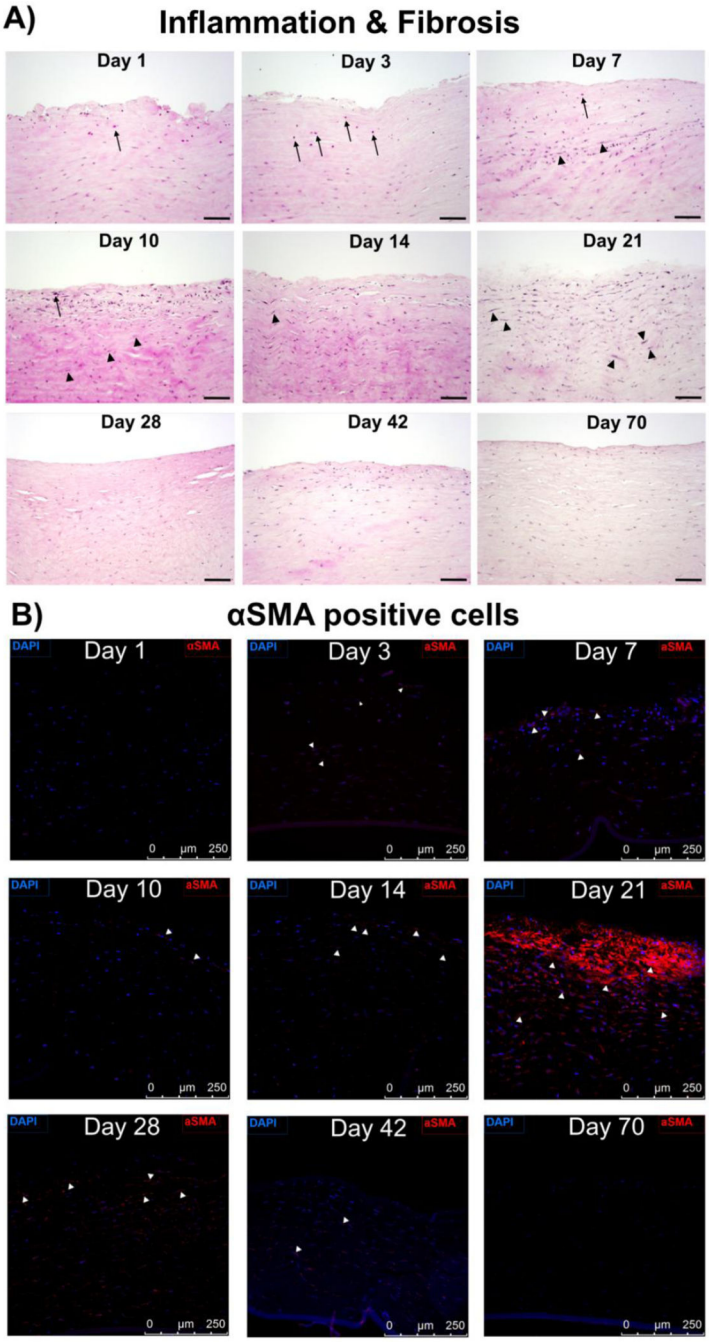

Figure 4.

Representative histologic images of a single field of view at each time point depicting **(A)** H&E stain to illustrate the presence of heterophils (indicated by black arrows, scale bar is 100 μm) typifying acute inflammation. Median scores for inflammation were 0 (none) for control eyes and on days 28, 42, 70; 1 (mild) on days 1, 7, 10, 14, 21; and 2 (moderate) on day 3. Median scores for fibrosis [indicated by increased fibroblast density (black arrowheads) and disorganized collagen (pink/eosinophilic matrix between nuclei)] were 0 (none) for control eyes and on days 1, 3; 1 (mild) on days 7, 28, 42; and 2 (moderate) on

days 10 and 21. **(B)** Presence of αSMA positive myofibroblasts (scale bar is 250 μm). Nuclei are stained by DAPI in blue, and myofibroblasts by αSMA in red. White arrows indicate representative αSMA positive cells. As demonstrated maximum number of myofibroblasts was evident on day 21 after wounding.

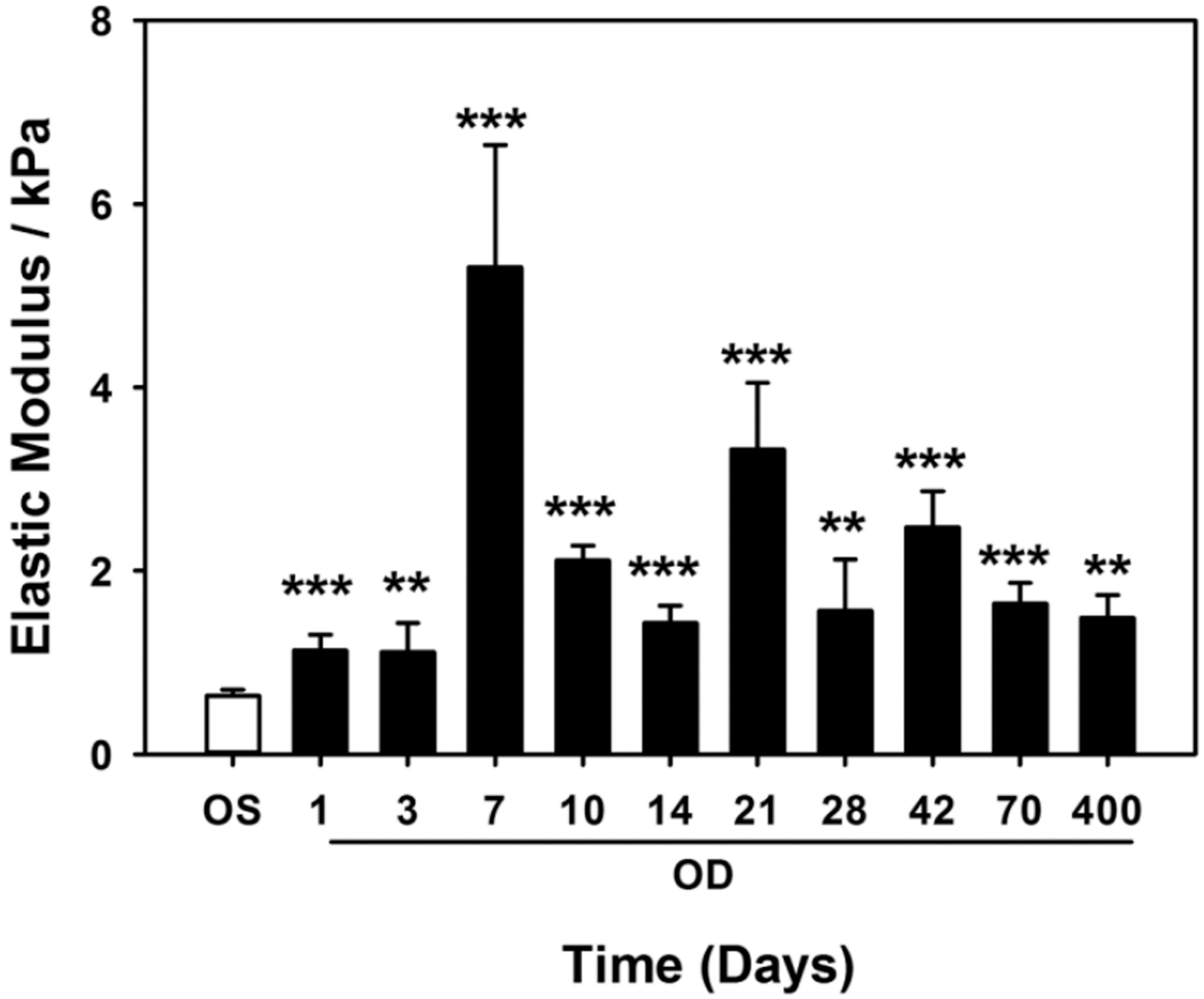

Figure 5.

Changes in elastic modulus throughout wound healing. Elastic modulus of the anterior stroma in wounded eyes (OD) increased to a maximum on day 7 after wounding. Subsequent changes in elastic moduli reflect the dynamic nature of wound repair and stromal remodeling. Measurements were obtained from 3 rabbits for each day up to 70 days, and for one rabbit on day 400. At each time point, modulus was also measured in the contralateral unwounded eye (OS). For each rabbit, force curves were obtained at 5 locations with at least 5 force curves obtained per location. Data are mean ± standard error in mean. **p<0.01, *** p<0.001, one-way ANOVA, followed by Dunnett's multiple comparison test compared with OS for each time point.

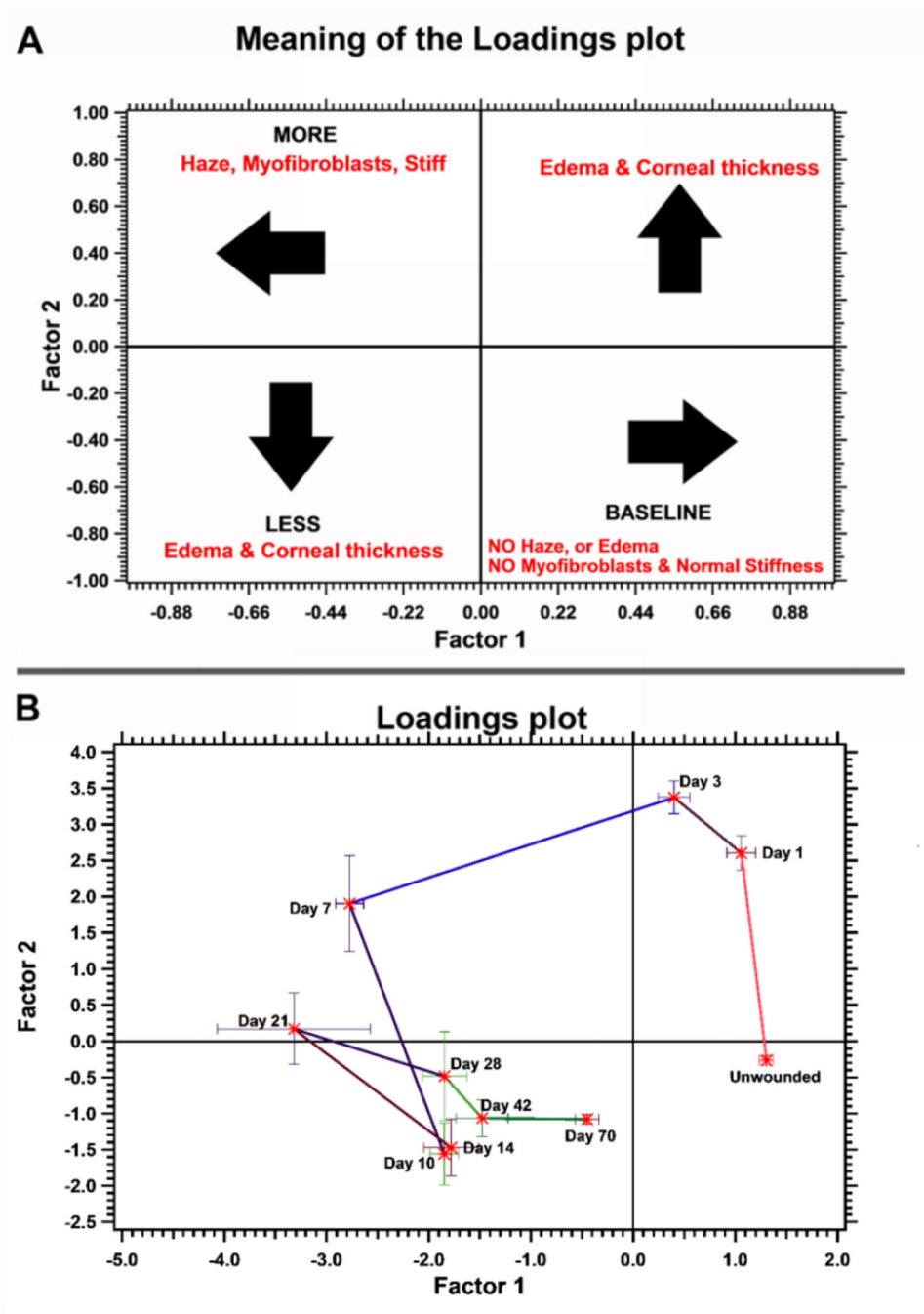

Figure 6.

Factor analysis and subsequent clustering reveal the different stages of wound healing. Factor analysis was performed with the data obtained (elastic modulus, inflammation, fibrosis, and edema scores, stromal haze and central corneal thickness, and number of αSMA positive cells). These were divided into two factors and the loadings plot explaining these factors are illustrated in **(A)**. The actual loadings plot for the data is provided in **(B)**. As observed, data are clustered for each time point and predict the changes in wound repair

parameters appropriately. The parameters between days 14 and 28 signify dynamic remodeling of the stroma.

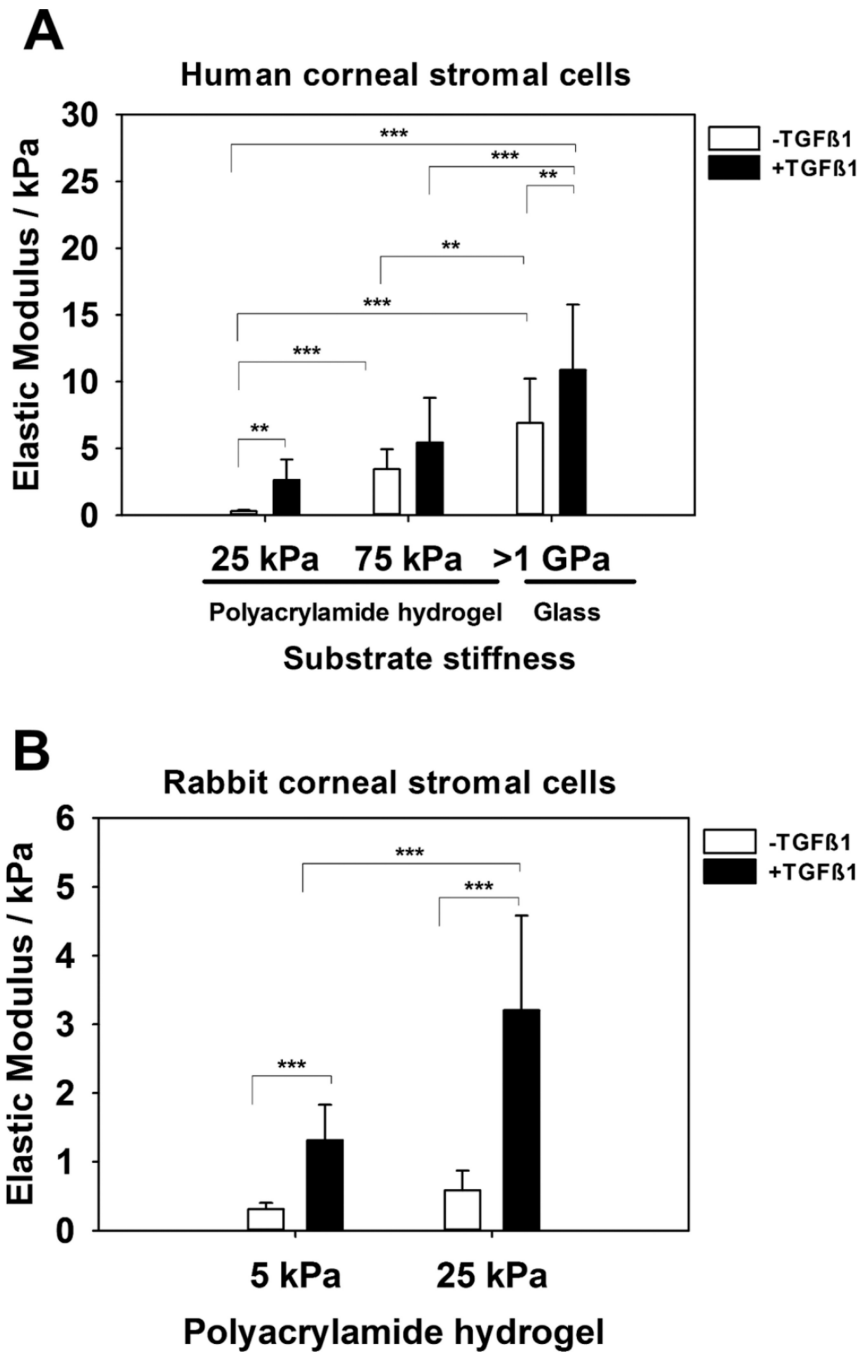

Figure 7.

Elastic modulus of corneal stromal cells as measured by AFM increases with substratum stiffness and the presence of TGFβ1. Elastic modulus of **(A)** human and **(B)** rabbit corneal stromal cells are dependent on the substrate they are cultured upon i.e. stiffer the substrate, stiffer the cells. TGFβ1 treated stromal cells are relatively stiffer than untreated cells. For each cell type, the experiment was repeated three times, and force curves were obtained over the nuclei of at least 5 cells with at least 5 force curves obtained per cell. Data represent the

mean ± standard error in mean. **p<0.01, *** p<0.001, one-way ANOVA, followed by Tukey's pairwise multiple comparison test.

Table 1

Measured parameters in no particular order that contribute to the two factors. The factors were interpreted by associating the variables with highest weights in each factor.

Factor 1	Factor 2
Elastic modulus	Central corneal thickness
αSMA positive cells (%)	Edema
Fibrosis	
Stromal haze thickness	